AGU PUBLICATIONS

Geophysical Research Letters

RESEARCH LETTER
10.1002/2017GL073442

Key Points:
- Level set approach to pressure- and saturation-controlled two-phase displacement at pore scale
- Pressure- and saturation-controlled capillary pressure curves differ significantly for drainage
- Spontaneous redistribution of fluids is more significant for drainage than imbibition

Supporting Information:
- Supporting Information S1

Correspondence to:
J. O. Helland,
joh@iris.no

Citation:
Helland, J. O., H. A. Friis, E. Jettestuen, and S. M. Skjæveland (2017), Footprints of spontaneous fluid redistribution on capillary pressure in porous rock, *Geophys. Res. Lett.*, *44*, 4933–4943, doi:10.1002/2017GL073442.

Received 13 MAR 2017
Accepted 16 MAY 2017
Accepted article online 18 MAY 2017
Published online 29 MAY 2017

Footprints of spontaneous fluid redistribution on capillary pressure in porous rock

Johan Olav Helland[1], Helmer André Friis[1], Espen Jettestuen[2], and Svein M. Skjæveland[3]

[1]International Research Institute of Stavanger, Stavanger, Norway, [2]International Research Institute of Stavanger, Oslo, Norway, [3]Department of Petroleum Engineering, University of Stavanger, Stavanger, Norway

Abstract Pore-scale imaging of two-phase flow in porous media shows that pore filling occurs as cooperative events with accompanying spontaneous fluid redistribution in other parts of the pore space. We present a level set method that controls saturation quasi-statically to model experiments controlled by low, constant flow rates and demonstrate that our method can describe the observed displacement mechanisms. The level set approach determines states of capillary equilibrium, which generally are different for displacement protocols constrained by saturation and pressure. Saturation-controlled simulations of drainage in sandstone show spontaneous fluid redistributions with abrupt pressure jumps and cooperative behavior, including snap-off and interface retraction events, consistent with experimental observations. Drainage capillary pressure curves are lower when saturation, rather than pressure, controls displacement. Remarkably, these effects are less significant for imbibition processes where the development of hydraulically connected wetting phase moderates the cooperative behavior and associated pressure jumps.

1. Introduction

Capillary pressure (P_c), defined as the pressure difference across interfaces between nonwetting phase (e.g., oil) and wetting phase (e.g., water), as a function of saturation (S), represents the action of capillary forces during two-phase flow in porous rock on the macroscopic (darcy) scale. This relationship exhibits hysteresis because it depends on the pore-scale fluid distribution, which in turn depends on the wetting state of the rock and the displacement history. On the pore scale, capillary forces usually dominate over gravity and viscous forces due to the small flow rates, length scales, and pore sizes involved [*Hilfer and Øren*, 1996]. Thus, it is natural to interpret $P_c(S)$ curves as a sequence of capillary-dominated pore-scale displacements representing transitions between local energy minima that occur in the form of alternate reversible and irreversible events, called "isons" and "rheons," respectively [*Morrow*, 1970; *Cueto-Felgueroso and Juanes*, 2016]. The standard simulation approach to such displacements is quasi-static methods that assume capillary forces alone control interface motion and approximate the process by a series of equilibrium states (local energy minima) at imposed capillary pressures [e.g., *Øren et al.*, 1998; *Hilpert and Miller*, 2001; *Jettestuen et al.*, 2013; *Xu and Louge*, 2015].

Recent pore-scale observations from X-ray microtomography images of two-phase capillary-dominated flow controlled by low, constant flow rates in porous rock [*Berg et al.*, 2013; *Andrew et al.*, 2015a; *Bultreys et al.*, 2015] have led to the conclusion that quasi-static pore-scale methods are insufficient to describe the fluid distributions arising from irreversible displacement events [*Armstrong and Berg*, 2013; *Armstrong et al.*, 2015; *Rücker et al.*, 2015; *Berg et al.*, 2016]. Here we introduce a new quasi-static simulation procedure that controls saturation to model displacement controlled by low rate in an existing level set method [*Jettestuen et al.*, 2013], accounting for capillary forces and wettability, and demonstrate that saturation-controlled simulations describe the essential displacement mechanisms observed in the above experiments, including irreversible events. Systematic pore-scale simulations on sandstone reveal that pressure- and saturation-controlled displacement protocols identify different series of capillary equilibrium states because the irreversible events behave differently in the two displacement modes, which generally result in different capillary pressure curves.

2. Pressure- and Saturation-Controlled Displacement

Reversible segments on the $P_c(S)$ curve (isons) occur with smooth changes of capillary pressure that are positive during drainage and negative during imbibition. Example displacements include piston-like invasion in straight capillary tubes, where work exerted on the fluid/rock system balances the change in interfacial free energy. The irreversible $P_c(S)$ segments (rheons) induce hysteresis [*Morrow*, 1970]. They represent spontaneous redistributions of fluid at almost constant saturation due to instabilities arising when an interface cannot change curvature smoothly with capillary pressure, resulting in abrupt pressure jumps. Haines jumps [*Haines*, 1930] refer to irreversible displacements that occur with saturation changes [*Morrow*, 1970]. Because saturation is constant during a rheon, external work is zero, while interfacial free energy is lost to heat and entropy increases, following the second law of thermodynamics [*Morrow*, 1970]. Therefore, only a fraction of the external work required for a drainage process in porous rocks converts into interfacial energy [*Seth and Morrow*, 2007; *Berg et al.*, 2013]. In drainage, rheons typically occur by sudden nonwetting phase invasion into larger pore regions, resulting in a temporary, abrupt capillary pressure drop that causes local imbibition events in nearby pore regions. This is known as cooperative behavior [*Morrow*, 1970; *Måløy et al.*, 1992; *Moebius and Or*, 2012]. Similarly, abrupt capillary pressure increases characterize rheons during imbibition. They can occur as a result of snap-off induced by swelling of wetting phase films [e.g., *Lenormand et al.*, 1983; *Deng et al.*, 2014], in which wetting phase invades the pore throat and displaces nonwetting phase to larger pore regions. Cooperative behavior during imbibition occurs as temporary drainage events in nearby pores.

The amount of cooperative behavior during a two-phase flow experiment depends on the boundary conditions [*Morrow*, 1970]. In this context it is useful to distinguish experiments controlled by pressure and saturation [*Cueto-Felgueroso and Juanes*, 2016]. *Pressure-controlled* experiments use a set of externally imposed capillary pressures, and for each pressure level the fluids relax to new equilibrium positions before the pressure level changes, consistent with standard methods for measuring $P_c(S)$ curves in porous rock. Because external phase pressures are fixed, the measured equilibrium $P_c(S)$ data are monotonic and do not contain traces of pressure jumps due to irreversible events, although recent experiments show that they do occur [*Moura et al.*, 2015, 2016]. *Moura et al.* [2015] measured pressure fluctuations at the outlet of the porous medium which was connected to a fluid reservoir with fixed pressure by a tubing that allows a viscous pressure gradient. At equilibrium, the pressure gradient vanishes and the measured pressure coincides with the equilibrium $P_c(S)$ data. Pressure-controlled displacement is also consistent with quasi-static pore network models [e.g., *Øren et al.*, 1998], based on invasion percolation [*Wilkinson and Willemsen*, 1983], and methods applied directly on segmented rock images [e.g., *Hilpert and Miller*, 2001; *Jettestuen et al.*, 2013], that assume capillary forces alone controls interface motion. *Saturation-controlled* (or rate-controlled) experiments typically uses a pump to withdraw or inject fluid at constant flow rate to carry out drainage or imbibition processes, while monitoring pressure at flow boundaries. If flow rate is sufficiently small, these experiments can be performed either quasi-statically or dynamically as an alternative and faster method to determine $P_c(S)$ curves. However, because such experiments control the invading volume of fluid, the $P_c(S)$ data can contain nonmonotonic pressure changes, indicating irreversible events with cooperative behavior [*Porter et al.*, 2010; *Herring et al.*, 2014; *Schlüter et al.*, 2016].

X-ray microtomography images of rate-controlled two-phase drainage experiments in porous rock show Haines jumps with cooperative behavior, including snap-off and coalescence events [*Berg et al.*, 2013; *Andrew et al.*, 2015a; *Bultreys et al.*, 2015]. Distant imbibition events, which occur as interface retraction and snap-off, supply nonwetting phase to large pore regions invaded during Haines jumps. These snap-off events can form temporary, disconnected nonwetting phase ganglia, whereas subsequent coalescence events reconnect most of these ganglia to the connected phase at later drainage stages [*Andrew et al.*, 2015a; *Singh et al.*, 2016]. Irreversible fluid redistributions like Haines jumps are clearly nonlocal mechanisms [*Morrow*, 1970; *Berg et al.*, 2013; *Andrew et al.*, 2015a], but their spatial extent, depending on pore geometry, fluid properties, and flow conditions [*Morrow*, 1970; *Armstrong and Berg*, 2013; *Armstrong et al.*, 2015], is difficult to determine. Haines jumps occur with sharp decreases of injection pressure [*Armstrong and Berg*, 2013; *Berg et al.*, 2013]. However, interface curvature of connected fluids before and after a Haines jump with significant pressure drop are spatially invariant, indicating two equilibrium states [*Andrew et al.*, 2015a]. Thus, capillary pressure gradients developed by a Haines jump dissipate rapidly after the event [*Armstrong and Berg*, 2013].

Irreversible events with cooperative behavior during imbibition is much less documented by pore-scale imaging techniques. *Rücker et al.* [2015] observed that snap-off events induce coalescence in nearby pore-space regions. Disconnected oil ganglia formed by snap-off events will move and deform until they reach a state of capillary equilibrium as determined by the local pore geometry. During this motion, they can merge with nearby ganglia, which in turn can induce further ganglion displacement toward other equilibrium positions. This snap-off/coalescence description shares similarities with drainage [*Berg et al.*, 2013] but contrasts with the work of *Andrew et al.* [2015b], who argued that imbibition occurs uniformly within the sample, by swelling of hydraulically connected wetting phase through a series of capillary equilibria. While snap-off occurs far away from equilibrium in drainage, for imbibition it is a more stable transition between two equilibrium configurations [*Andrew et al.*, 2015b]. Depending on pore geometry, snap-off processes can also induce wetting phase invasion into larger regions containing several throats [*Rücker et al.*, 2015], possibly accompanied by cooperative events before reaching equilibrium.

Dynamic two-phase flow simulations based on the Navier-Stokes equations, including viscous, inertial, and capillary forces, provide insights into the displacement mechanisms observed in the rate-controlled experiments described above. For example, *Zacharoudiou and Boek* [2016] simulated Haines jumps with cooperative effects during drainage using a lattice-Boltzmann method. We propose that the constraints on invading fluid volumes is responsible for a major part of the cooperative behavior observed in experiments controlled by low, constant flow rates and that quasi-static methods for saturation-controlled displacement can describe the main features of evolving fluid distributions in such experiments. We use a level set method previously developed for pressure-controlled displacement [*Jettestuen et al.*, 2013], modified here to include displacements controlled by saturation. We compare pressure- and saturation-controlled simulations on sandstone and find substantial differences in $P_c(S)$ curves and evolving fluid distributions during drainage, which we explain by significant cooperative effects in the saturation-controlled case. The two approaches show much more similar results for imbibition because development of hydraulically connected wetting phase moderates the cooperative effects and associated capillary pressure jumps.

3. Level Set Method

We assume quasi-static, capillary-controlled displacement at the pore scale, such that all interfaces satisfy the Young-Laplace equation:

$$P_c = \sigma C, \tag{1}$$

at equilibrium. Here σ is interfacial tension, and C is interface curvature.

In the level set (LS) method presented by *Jettestuen et al.* [2013], an implicit function ϕ represents oil/water interfaces as $\phi = 0$, with $\phi > 0$ in water (wetting phase) and $\phi < 0$ in oil (nonwetting phase). Curvature κ relates directly to the LS function ϕ through $\kappa = \nabla \cdot \nabla\phi/|\nabla\phi|$. At capillary equilibrium, κ equals C only at the interfaces ($\phi = 0$). A static LS function ψ describes pore/solid interfaces by $\psi = 0$, where $\psi > 0$ in pore space and $\psi < 0$ in solid. The evolution equation for ϕ uses a stepwise velocity to distinguish interface motion in pore space from contact angle formation on pore walls (with extension into solid) [*Jettestuen et al.*, 2013]:

$$\phi_t + H(\psi)\,(C - \kappa)\,|\nabla\phi| + \frac{H(-\psi)}{\Delta x} S(\psi)\,(\nabla\phi \cdot \nabla\psi - \cos\beta |\nabla\phi||\nabla\psi|) = 0. \tag{2}$$

Here $H(\cdot)$ is a Heaviside step function that separates pore and solid velocities, and $S(\cdot)$ is a sign function. With our sign convention for the level set functions, β is the intersection angle between contours of ϕ and ψ, measured through oil. It relates to contact angle θ, measured through water, by $\theta = 180° - \beta$. We solve equation (2) iteratively using explicit numerical schemes with reflective (Neumann) boundary conditions, except at inlet, where we use linear extrapolation. At inlet, we also add a pore-space layer filled with oil (for oil invasion) or a water-wet porous plate saturated with water (for water invasion). *Jettestuen et al.* [2013] describe the implementation details. Steady state solutions ($\phi_t = 0$) correspond to equilibrium fluid configurations, which occur when the zero contour ($\phi = 0$) satisfies equation (1) in pore space while contact angle forms on the pore walls and in solid. That is,

$$C = \kappa \quad \text{and} \quad \cos\beta = \frac{\nabla\phi}{|\nabla\phi|} \cdot \frac{\nabla\psi}{|\nabla\psi|}. \tag{3}$$

Pressure-controlled displacement uses a specified sequence of interface curvatures $C_k = C_1 + (k-1)\Delta C$, $k = 1, \ldots, m$ that relate to capillary pressures $P_{c,k}$ through equation (1), where m is the number of $P_c(S)$ data

points. For each capillary pressure, we solve equation (2) and calculate saturation based on the obtained steady state solution for ϕ, which we take as input to the next pressure level. *Jettestuen et al.* [2013] validated this approach numerically.

Saturation-controlled displacement specifies oil saturations $S_{o,k} = S_{o,1} + (k-1)\Delta S_o$, $k = 1, \ldots, m$, which correspond to target oil volumes $V_{o,k}^{\text{target}} = S_{o,k} V_p$, where V_p is pore volume. For each input saturation, this approach calculates pressure (or, equivalently, interface curvature C) in each iteration step with equation (2), following *Saye and Sethian* [2011]:

$$C^n = \frac{V_o^{\text{target}} - V_o^n}{\Delta t A_{\text{ow}}^n}, \tag{4}$$

where we omit index k for clarity. In equation (4), V_o^n is the oil volume and A_{ow}^n is the oil/water interfacial area in iteration step n, and Δt is the iteration time step. Equation (4) updates interface curvature C to control shrinkage or growth of the oil phase in the normal direction around its boundary during evolution of ϕ toward the target oil volume. We take the converged solution of ϕ, which satisfies equation (3), as input to the next saturation step. Section S1 and Figures S1–S4 in the supporting information shows a numerical validation of the saturation-controlled approach. Recently, we used equation (4) to preserve volumes of an isolated oil ganglion surrounded by water and gas during three-phase displacement in porous rock [*Helland and Jettestuen*, 2016]. Equation (4) controls entire phase volumes. Extending its use to preserve different ganglia volumes locally, through fragmentation and coalescence processes, is work in progress.

We calculate oil volume V_o, oil/water and oil/solid interfacial areas, A_{ow} and A_{os}, respectively, by volume integrals over the computational domain D:

$$V_o = \int_D H(\psi) H(-\phi) \mathrm{d}V, \tag{5}$$

$$A_{\text{ow}} = \int_D H(\psi) \delta(\phi) |\nabla \phi| \mathrm{d}V, \tag{6}$$

and

$$A_{\text{os}} = \int_D H(-\phi) \delta(\psi) |\nabla \psi| \mathrm{d}V, \tag{7}$$

where $\delta(\cdot)$ is the delta function. Specific oil/water interfacial area is defined as $a_{\text{ow}} = A_{\text{ow}}/V_p$.

4. Results

We study a porous rock geometry extracted from a freely available segmented tomography data set of Castlegate sandstone with voxel length 5.6 μm [*Sheppard*, 2015]. The subset has porosity 29% and contains $200 \times 200 \times 200$ voxels, corresponding to a cube with side lengths 1.1 mm. We use contact angle $\theta = 20°$, describing a water-wet state, and assume interfacial tension is 0.030 N/m. We implemented our LS code within the SAMRAI software framework [*Hornung and Kohn*, 2002; *Hornung et al.*, 2006] and ran all simulations as parallel jobs at the national e-infrastructure for high-performance computing in Norway, using 350 CPUs. Average simulation run time was around 7 h.

For drainage, the saturation-controlled simulations with $\Delta S_o = 0.005, 0.01, 0.02$, and 0.04 all exhibit nonmonotonic $P_c(S)$ curves, consisting of alternate saturation intervals with abrupt P_c drops (rheons) and gradual P_c increases (isons), see Figure 1 (left column, top). In our method, these P_c changes occur uniformly over the sample. Figure 1 (right column, top and middle) shows examples of typical spontaneous fluid redistributions (rheons) with cooperative behavior that occur in our simulations. Oil invades larger pore regions by Haines jumps, while neighboring oil regions coalesce in some of the narrow pore throats. Simultaneously, temporary imbibition processes occur uniformly within the sample in the form of interface retraction and snap-off, consistent with experimental observations [*Berg et al.*, 2013; *Rücker et al.*, 2015; *Andrew et al.*, 2015a]. For the drainage processes, we also observe that snap-off events can occur multiple times in the same location during different rheons, separated by alternate coalescence events in other saturation intervals. In agreement with experiments [*Armstrong and Berg*, 2013], interface oscillation with temporary pore drainage/imbibition events occurs as the fluids relax toward equilibrium at the target saturation. During drops of P_c, interfacial area A_{ow} increases abruptly due to interface retraction events, see Figure 1 (left column, top and middle). This leads to more modest increases of A_{os} than observed for P_c increments and sometimes even decreased A_{os}.

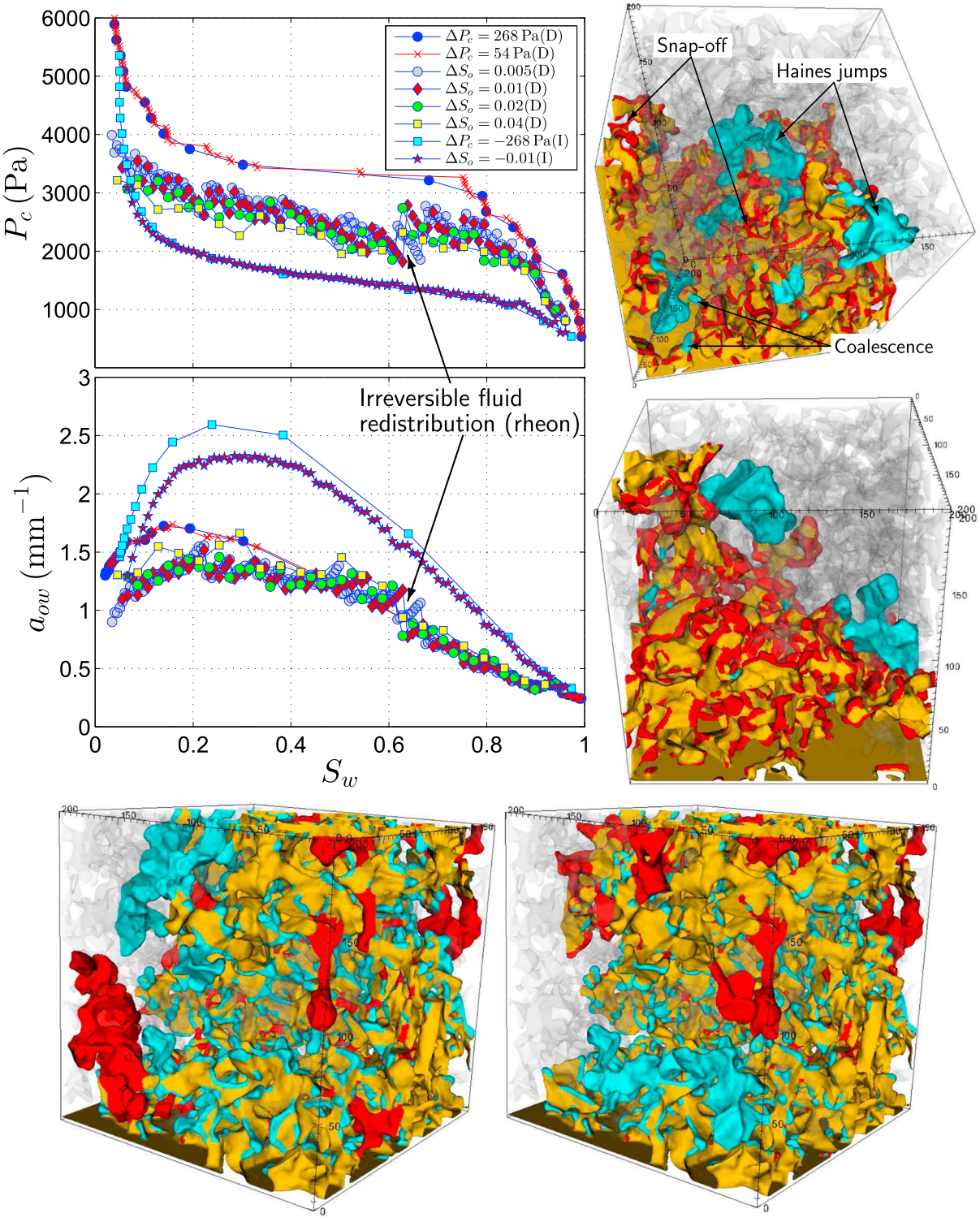

Figure 1. (left column) Capillary pressure (top) and specific interfacial area (middle) as function of water saturation for pressure-controlled and saturation-controlled simulations of primary drainage (*D*) and imbibition (*I*) in Castlegate sandstone. The imbibition processes use fluid configurations at $S_{wi} = 0.05$ from the drainage processes with corresponding pressure and saturation steps as input. Oil invasion occurs through bottom boundary, and water invasion occurs through top boundary. (right column) Drainage oil configurations compared before (in yellow and red) and after (in yellow and blue) the irreversible fluid redistribution associated with the abrupt capillary pressure drop indicated on the left plots, for the drainage simulations with $\Delta S_o = 0.04$ (top) and $\Delta S_o = 0.01$ (middle). (bottom row) Drainage oil configurations at $S_w = 0.3$ from the pressure-controlled displacement (in yellow and blue), with $\Delta P_c = 268$ kPa and the saturation-controlled displacements (in yellow and red), with $\Delta S_o = 0.04$ (left) and $\Delta S_o = 0.01$ (right).

The $P_c(S)$ curves from the pressure-controlled simulations are monotonic and consist of irreversible saturation jumps at fixed capillary pressure connected by smaller reversible saturation intervals with more steeply increasing capillary pressure. These features become visible for small pressure steps ΔP_c, see Figure 1 (left column, top). The pressure-controlled simulations assume displacement at fixed capillary pressure and do not exhibit pressure drops or cooperative behavior.

Figure 1 (left column, top) shows that the pressure-controlled displacement exhibits higher pressure level than the displacement controlled by saturation. We interpret this as effects of displacement histories that develop differently for the two displacement protocols. Thus, the series of local energy minima obtained with equation (2) for processes constrained by pressure and saturation are different. Figure 1 (bottom row) shows significant differences between oil configurations for pressure- and saturation-controlled simulations at water saturation $S_w = 0.3$. In addition to the different large pore regions invaded by oil, the main trend is that oil-filled pores contain larger amounts of water in pore corners in the saturation-controlled cases because P_c is smaller. However, more coalescence events in the saturation-controlled case fills more pore throats with oil, connecting larger oil regions. *Armstrong et al.* [2016] showed that the Euler characteristic describes effectively the amount of coalescence events and fluid connectivity. Figure 1 (bottom row) shows that oil configurations in saturation-controlled simulations with $\Delta S_o = 0.01$ and 0.04 also differ significantly due to differences in the history of displacements. Although the most accurate approach is to use small ΔS_o to determine always the nearest energy minimum to the current state, we cannot choose ΔS_o such that only one distinct displacement occurs in each saturation interval. However, Figure 1 (right column, top and middle) shows that the size of Haines jumps in terms of invaded pores is about the same for $\Delta S_o = 0.01$ and 0.04. The main differences are that more Haines jumps, less significant temporary imbibition processes in oil-invaded regions, and smaller pressure drops, occur when saturation step is larger. As ΔS_o approaches zero, we approximate rheons, which occur at constant saturation, resulting in more abrupt pressure drops and energy loss [*Morrow*, 1970]. Large ΔS_o contains a combination of reversible and irreversible events that cumulatively result in a smaller pressure drop. For $\Delta S_o = 0.005$, 0.01, and 0.02 most of the pressure drops are larger than 100 Pa (the largest pressure jump, indicated in Figure 1, is 985 Pa), while for $\Delta S_o = 0.04$, most pressure drops are smaller than 100 Pa. These magnitudes agree with previously reported values from experiments in porous rock [*Berg et al.*, 2013; *Andrew et al.*, 2015a].

In a subsequent saturation-controlled imbibition process with initial water saturation $S_{wi} = 0.05$ and $\Delta S_o = -0.01$, abrupt pressure jumps and cooperative behavior are remarkably smaller, see Figure 1 (left column, top). The $P_c(S)$ data follow the curve from the corresponding pressure-controlled simulation. In our method, we assume that the initial water phase present in pore corners and narrow pore throats after drainage is hydraulically connected and in contact with the invading water through thin films. For these conditions, we propose that water invasion through films is significant and results in uniform swelling of the water phase throughout the sample. A sequence of capillary equilibria corresponding to smoothly decreasing capillary pressures describe both this process and the snap-off events in pore throats [*Andrew et al.*, 2015b]. Figure 1 (left column, middle) shows that uniform water swelling results in higher interfacial area for imbibition than drainage, contrary to measured data on sphere packs where imbibition happens by frontal advance [*Porter et al.*, 2010; *Schlüter et al.*, 2016].

To investigate if it is the initial water content that moderates the pressure jumps and cooperative behavior during imbibition, we simulate a similar imbibition process without water present in the sample initially. In this case, water invasion for small S_w occurs by development of films, through which water fills pore corners and throats ahead of the frontal advance. For S_w larger than about 0.55, an approximately uniform distribution of water has developed throughout the sample, which moderates the cooperative behavior. Figure 2 (left column, top) shows that much more significant P_c increments, larger than 100 Pa, occur when $S_w < 0.55$. At higher water saturations, the pressure jumps are smaller than 50 Pa, as for the imbibition with $S_{wi} = 0.05$. Figure 2 (right column, top) shows the spontaneous fluid redistribution associated with the largest pressure increase (about 250 Pa) for the imbibition process without water present initially. Water saturation here is about 0.25. While snap-off events fill individual pore throats with water, we also observe that snap-off can result in water invasion into larger regions containing many throats [*Rücker et al.*, 2015]. The associated cooperative behavior occurs uniformly throughout the sample as temporary drainage processes where interfaces move farther into pore corners and reduces the water content there. We expect that these processes can result in coalescence events that fill pore throats with oil [*Rücker et al.*, 2015], although we do not observe such events in our imbibition simulations. Figure 2 (bottom row) shows that more significant differences

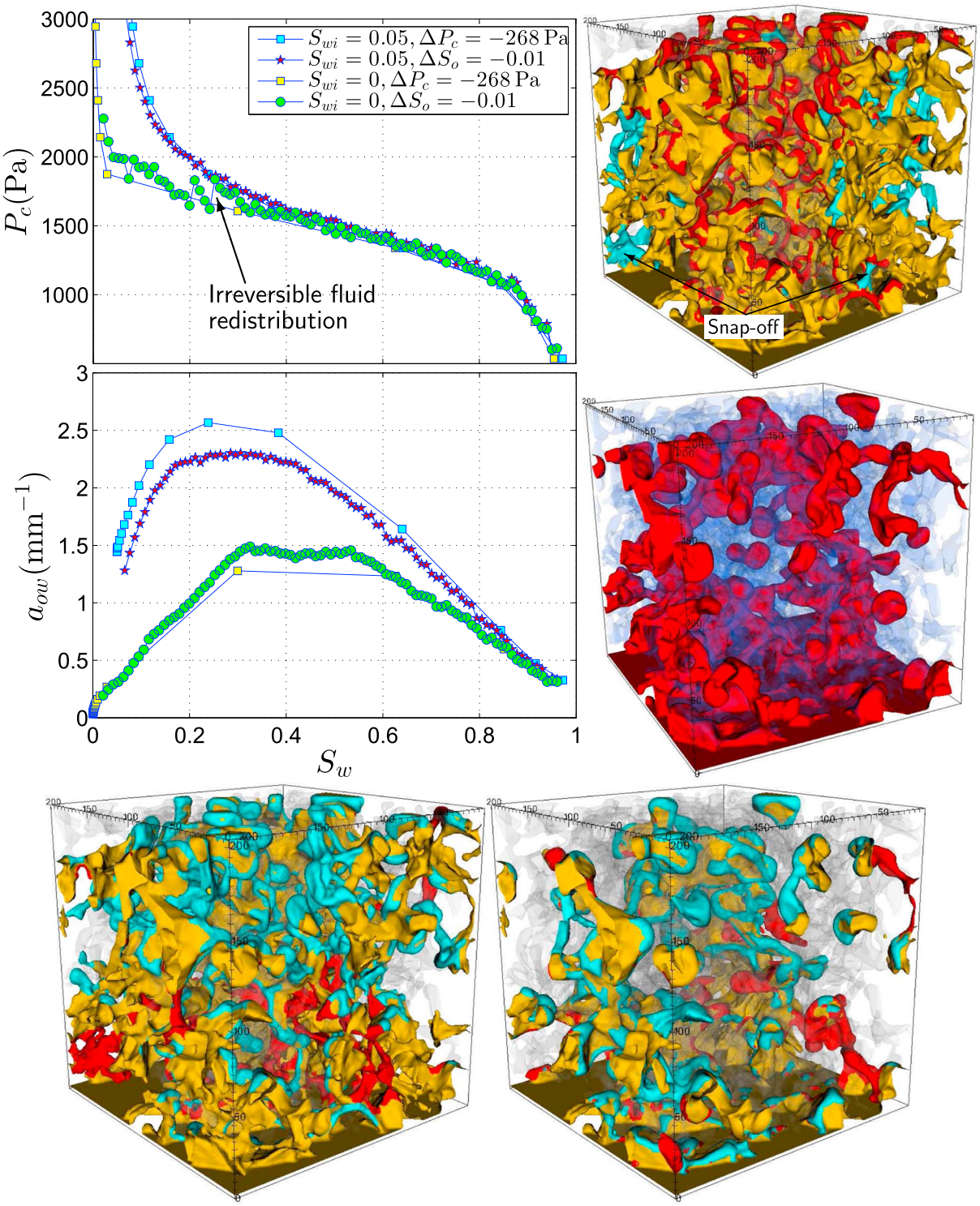

Figure 2. (left column) Capillary pressure (top) and specific interfacial area (middle) as function of water saturation for pressure-controlled and saturation-controlled simulations of imbibition processes in Castlegate sandstone with and without water present initially. (right colum) Top: Imbibition oil configurations compared before (in yellow and blue) and after (in yellow and red) the irreversible fluid redistribution associated with the abrupt capillary pressure increase indicated on the left plot, for the saturation-controlled imbibition simulation with $S_{wi} = 0$. (right column) Middle: Oil (red) and water (transparent blue) configuration at $S_w = 0.6$ from the saturation-controlled imbibition with $S_{wi} = 0.05$. Water invasion occurs through top boundary. (bottom row) Imbibition oil configurations from the pressure-controlled displacement (in yellow and red) and the saturation-controlled displacement (in yellow and blue), at $S_w = 0.3$ (left) and $S_w = 0.62$ (right), for the imbibition processes without water present initially ($S_{wi} = 0$).

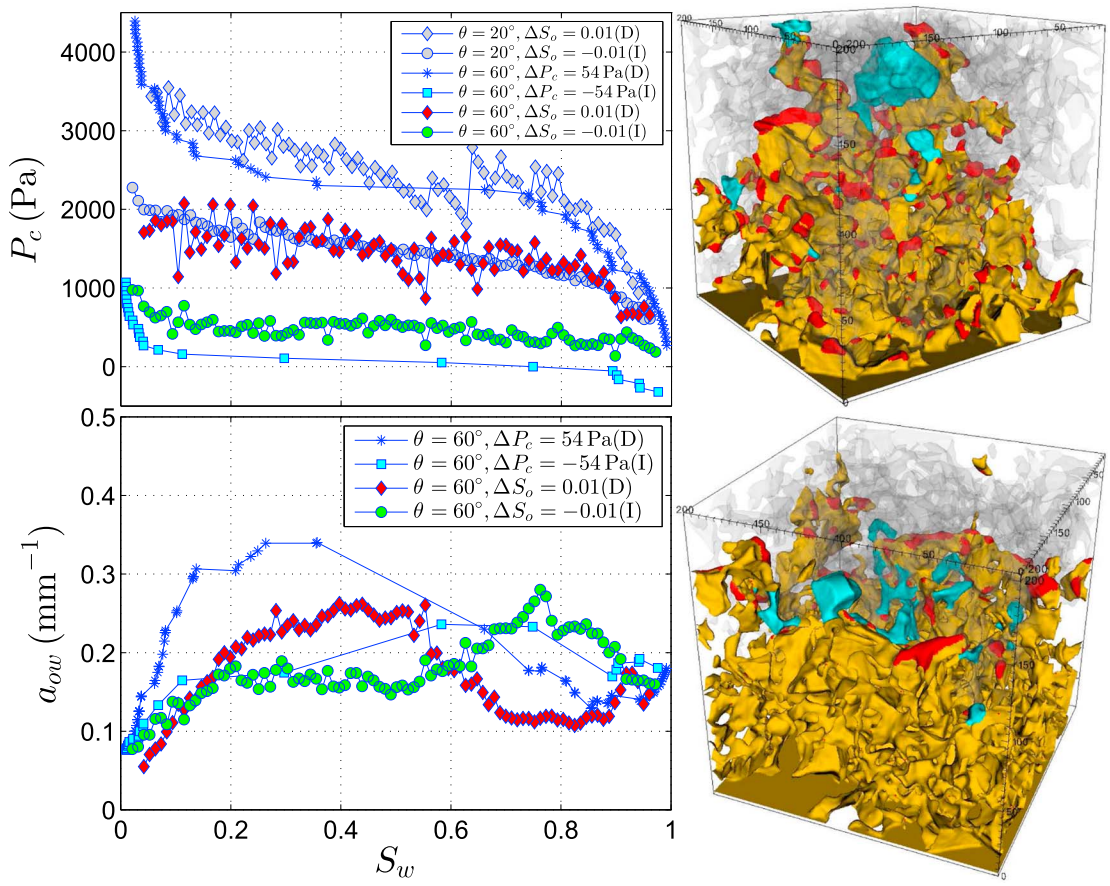

Figure 3. (top left) Capillary pressure and (bottom left) specific interfacial area as function of water saturation for pressure-controlled and saturation-controlled simulations of primary drainage (*D*) and imbibition (*I*) in Castlegate sandstone with $\theta = 60°$. The imbibition processes occur without water present in the sample initially. (top right) Oil configurations in the saturation-controlled drainage with $\theta = 60°$ before (in yellow and red) and after (in yellow and blue) the capillary pressure drop at $S_w = 0.56$. (bottom right) Oil configurations in the saturation-controlled imbibition with $\theta = 60°$ before (in yellow and blue) and after (in yellow and red) the capillary pressure jump at $S_w = 0.38$. Oil invasion occurs through bottom boundary, and water invasion occurs through top boundary.

between the pressure- and saturation-controlled simulations occur for small water saturations. Because P_c is slightly higher in the saturation-controlled case, more water is present in corners of oil-filled pores in the pressure-controlled configuration. However, our results suggest that pressure-controlled displacements approximate saturation-controlled displacements when the wetting phase initially is hydraulically connected within the sample.

To investigate wettability effects on the pressure- and saturation-controlled displacement protocols, we perform simulations with $\theta = 60°$. Figure 3 (left column, top) shows that these results display a more symmetric behavior between drainage and imbibition than the simulations with $\theta = 20°$. The saturation-controlled $P_c(S)$ curve for drainage is still lower than the pressure-controlled curve, whereas for imbibition, the saturation-controlled $P_c(S)$ curve now occurs at a higher pressure level than the pressure-controlled curve. In the pressure-controlled displacement, spontaneous imbibition ceases at $S_w = 0.75$ and forced imbibition continues with negative capillary pressure. While the drainage processes show similar behavior as for $\theta = 20°$, see Figure 3 (right column, top), the imbibition processes with $\theta = 60°$ occurs by frontal advance and piston-like invasion without water-film development. The saturation-controlled imbibition exhibits more significant pressure jumps during the entire process than the imbibition with $\theta = 20°$, and the corresponding cooperative behavior is restricted to the imbibing front, see Figure 3 (right column, bottom). However, still the pressure jumps are smaller for imbibition than for drainage. We explain this as follows: In drainage, equilibrium interface positions occur at the entrance to pore throats where capillary pressure can vary significantly depending on cross-sectional throat radius and the precise interface location. In imbibition, interfaces imbibe pore throats and relax to equilibrium positions within wider pore regions where capillary pressure

is always small. Because imbibition occurs by frontal advance, interfacial area is smaller for imbibition than for drainage in most of the saturation range, consistent with sphere-pack measurements [*Porter et al.*, 2010; *Schlüter et al.*, 2016].

The efficiency (E_d) of converting external work (W) to increase in interfacial free energy of the fluid/rock system (ΔF) for a drainage process to oil saturation S_o^* is [*Morrow*, 1970]

$$E_d[\%] = \frac{\Delta F}{W} \times 100 = \frac{\sigma(\Delta A_{ow} + \Delta A_{os}\cos\theta)}{V_p \int_0^{S_o^*} P_c \mathrm{d}S_o} \times 100. \quad (8)$$

For the drainage processes with $\theta = 20°$, the pressure-controlled displacement with $\Delta P_c = 268$ Pa, from beginning to $S_w = 0.2$ and 0.05, obtains $E_d = 54.2\%$ and 53.8%, respectively. For the corresponding saturation-controlled process with $\Delta S_o = 0.01$, these efficiencies are $E_d = 70.6\%$ and 70.3%. The saturation-controlled process converts work to energy more efficiently because the capillary pressures are smaller. Thus, we expect smaller hysteresis between drainage and imbibition in experiments controlled by saturation, consistent with Figure 1 (left column, top). Inspection of each saturation step shows a decrease of interfacial energy (that characterizes rheons) only for the spontaneous redistribution event highlighted in Figure 1 (left column, top). The energy decreases with 84% of the external work required to change saturation 1%. Hence, the efficiency for this event is negative (−84%). However, most saturation intervals contain both reversible events and irreversible events with varying cooperative effects. Thus, a major part of the saturation intervals, with positive and negative pressure jumps, exhibit efficiencies within the same range (see section S2 and Figure S5 in the supporting information). *Seth and Morrow* [2007] showed that E_d depends on pore body-to-throat aspect ratio. High aspect ratio gives more snap-off events during imbibition, which can lead to more trapping of oil. For drainage processes, it is possible that more snap-off events occur as part of the cooperative behavior during an irreversible fluid redistribution for high aspect ratio, which can decrease the efficiency of work conversion to energy. For drainage processes to $S_w = 0.2$, *Seth and Morrow* [2007] estimated $E_d = 36\%$ for Berea sandstone with aspect ratio between 4 and 6.7 and $E_d = 85\%$ for sphere packs with aspect ratio between 1.47 and 2.67. This is consistent with the efficiencies we calculate for Castlegate sandstone, for which average aspect ratio is 2.9 [*Knackstedt et al.*, 2006].

The saturation-controlled approach presented here captures the variations of capillary pressure with interface curvature as the interfaces move through wide and narrow pore regions, while the pressure-based approach does not. Thus, we can argue that the saturation-controlled approach is more consistent with the definition of capillary pressure. It also shares similarities with a method recently proposed by *McClure et al.* [2017] for calculating and measuring capillary pressure. They generated random fluid distributions in porous media for the entire saturation range and used a lattice Boltzmann method to calculate equilibrium fluid distributions and capillary pressure for each case based on averaged interface curvatures. The resulting capillary pressure curve was significantly lower than that obtained with externally imposed phase pressure differences during fluid invasion through an inlet boundary. These results conform with our saturation- and pressure-based simulations; see Figure 1 (left column, top).

Because fluid configurations and capillary pressure curves obtained under pressure- and saturation-controlled conditions generally are different, it is important to understand which of the two displacement protocols are most relevant in applications. For a representative porous rock volume within a reservoir far away from wells, pressure controls fluid displacement, whereas flow-rate controlled experiments performed on small rock samples comply with saturation-controlled conditions. The steady state method for estimating relative permeability belongs to the latter category because fixed fractional flows control the injection of each fluid toward constant saturations and pressures [e.g., *Alizadeh and Piri*, 2014]. Thus, quasi-static, pressure-controlled methods for estimating capillary pressure curves may produce fluid configurations that are incompatible with that obtained in rate-controlled relative permeability measurements [*Berg et al.*, 2016]. Obviously, a consistent utilization of capillary pressure and relative permeability data requires that they are measured for the same process with equal flow constraints imposed.

5. Conclusion

A quasi-static level set method which controls saturation, rather than capillary pressure, captures the essential displacement mechanisms observed in pore-scale experiments of two-phase drainage controlled by low, constant flow rates. The displacements occur as alternate reversible and irreversible events, previously

described based on thermodynamics [*Morrow*, 1970; *Cueto-Felgueroso and Juanes*, 2016]. Our method uses small saturation steps to approach irreversible events at constant saturation. These events are spontaneous fluid redistributions with abrupt pressure drops that include oil invasion into large pore regions and coalescence events. Simultaneously, cooperative effects in the form of temporary imbibition processes, such as interface retraction and snap-off, occur uniformly within the sample. The abrupt pressure drops result in an increase of oil/water interfacial area, at the expense of a more moderate increase, or even decrease, of oil/solid interfacial area. Drainage capillary pressure for pressure-controlled displacements is higher than for saturation-controlled displacements. Therefore, saturation-controlled displacements are more energy efficient and lead to smaller hysteresis between drainage and imbibition. During imbibition, uniform swelling of a hydraulically connected water phase throughout the porous rock moderates the cooperative effects significantly as compared to drainage. Transitions between capillary equilibria with monotonically decreasing capillary pressures describe these imbibition processes. Consequently, saturation- and pressure-controlled imbibition displacements approach each other. However, if the initial water present in the rock is hydraulically disconnected from the invading water, we expect that irreversible events with significant cooperative behavior can occur during imbibition. For weakly water-wet conditions, imbibition occurs by frontal advance without water-film swelling, which results in a more symmetric behavior between drainage and imbibition in terms of pressure jumps and cooperative behavior. In this case, saturation-controlled imbibition exhibits a higher capillary pressure level than pressure-controlled imbibition.

Acknowledgments
Financial support was provided by the Research Council of Norway under Petromaks2 project 234131/E30 "Three-phase capillary pressure, hysteresis, and trapping in mixed-wet rock" and ConocoPhillips through the research center COREC. The computations were performed on resources provided by UNINETT Sigma2—the National Infrastructure for High Performance Computing and Data Storage in Norway. The rock image data used in this paper are properly cited and referred to in the reference list. All other numerical information is provided in the figures produced by solving the equations described in the paper.

References

Alizadeh, A. H., and M. Piri (2014), Three-phase flow in porous media: A review of experimental studies on relative permeability, *Rev. Geophys.*, *52*, 468–521, doi:10.1002/2013RG000433.

Andrew, M., H. Menke, M. J. Blunt, and B. Bijeljic (2015a), The imaging of dynamic multiphase fluid flow using synchrotron-based X-ray microtomography at reservoir conditions, *Transp. Porous Media*, *110*, 1–24, doi:10.1007/s11242-015-0553-2.

Andrew, M., H. Menke, M. J. Blunt, and B. Bijeljic (2015b), Dynamic drainage and imbibition imaged using fast X-ray microtomography, paper SCA2015-009 presented at the International Symposium of the Society of Core Analysts, 12 pp., St. John's, Newfoundland, 16–21 Aug.

Armstrong, R., and S. Berg (2013), Interfacial velocities and capillary pressure gradients during Haines jumps, *Phys. Rev. E*, *88*(4), 043010, doi:10.1103/PhysRevE.88.043010.

Armstrong, R. T., N. Evseev, D. Koroteev, and S. Berg (2015), Modeling the velocity field during Haines jumps in porous media, *Adv. Water Resour.*, *77*, 57–68, doi:10.1016/j.advwatres.2015.01.008.

Armstrong, R. T., J. McClure, M. A. Berrill, M. Rücker, S. Schlüter, and S. Berg (2016), Beyond Darcy's law: The role of phase topology and ganglion dynamics for two-fluid flow, *Phys. Rev. E*, *94*(4), 043113, doi:10.1103/PhysRevE.94.043113.

Berg, S., et al. (2013), Real-time 3D imaging of Haines jumps in porous media flow, *Proc. Natl. Acad. Sci. U.S.A.*, *110*(10), 3755–3759, doi:10.1073/pnas.1221373110.

Berg, S., et al. (2016), Connected pathway relative permeability from pore-scale imaging of imbibition, *Adv. Water Resour.*, *90*, 24–35, doi:10.1016/j.advwatres.2016.01.010.

Bultreys, T., M. A. Boone, M. N. Boone, T. De Schryver, B. Masschaele, D. Van Loo, L. Van Hoorebeke, and V. Cnudde (2015), Real-time visualization of Haines jumps in sandstone with laboratory-based microcomputed tomography, *Water Resour. Res.*, *51*, 8668–8676, doi:10.1002/2015WR017502.

Cueto-Felgueroso, L., and R. Juanes (2016), A discrete-domain description of multiphase flow in porous media: Rugged energy landscapes and the origin of hysteresis, *Geophys. Res. Lett.*, *43*, 1615–1622, doi:10.1002/2015GL067015.

Deng, W., M. B. Cardenas, and P. C. Bennett (2014), Extended Roof snap-off for a continuous nonwetting fluid and an example case for supercritical CO_2, *Adv. Water Resour.*, *64*, 34–46, doi:10.1016/j.advwatres.2013.12.001.

Haines, W. B. (1930), Studies in the physical properties of soils. The hysteresis effect in capillary properties, and modes of moisture distribution associated therewith, *J. Agric. Sci.*, *20*, 97–116, doi:10.1017/S002185960008864X.

Helland, J. O., and E. Jettestuen (2016), Mechanisms for trapping and mobilization of residual fluids during capillary-dominated three-phase flow in porous rock, *Water Resour. Res.*, *52*, 5376–5392, doi:10.1002/2016WR018912.

Herring, A. L., L. Andersson, D. L. Newell, J. W. Carey, and D. Wildenschild (2014), Pore-scale observations of supercritical CO_2 drainage in Bentheimer sandstone by synchrotron X-ray imaging, *Int. J. Greenhouse Gas Control*, *25*, 93–101, doi:10.1016/j.ijggc.2014.04.003.

Hilfer, R., and P. E. Øren (1996), Dimensional analysis of pore scale and field scale immiscible displacement, *Transp. Porous Media*, *22*, 53–72.

Hilpert, M., and C. T. Miller (2001), Pore-morphology-based simulation of drainage in totally wetting porous media, *Adv. Water Resour.*, *24*, 243–255.

Hornung, R. D., and S. R. Kohn (2002), Managing application complexity in the SAMRAI object-oriented framework, *Concurr. Comput. Pract. E.*, *14*, 347–368. [Available at http://www.llnl.gov/CASC/SAMRAI.]

Hornung, R. D., A. M. Wissink, and S. R. Kohn (2006), Managing complex data and geometry in parallel structured AMR applications, *Eng. Comput.*, *22*, 181–195.

Jettestuen, E., J. O. Helland, and M. Prodanović (2013), A level set method for simulating capillary-controlled displacements at the pore scale with nonzero contact angles, *Water Resour. Res.*, *49*, 4645–4661, doi:10.1002/wrcr.20334.

Knackstedt, M., et al. (2006), 3D imaging and flow characterization of the pore space of carbonate core samples, paper SCA2006-023 presented at the International Symposium of the Society of Core Analysts, 13 pp., Trondheim, Norway, 12–16 Sep.

Lenormand, R., C. Zarcone, and A. Sarr (1983), Mechanisms of the displacement of one fluid by another in a network of capillary ducts, *J. Fluid Mech.*, *135*, 337–353, doi:10.1017/S0022112083003110.

McClure, J. E., A. L. Dye, C. T. Miller, and W. G. Gray (2017), On the consistency of scale among experiments, theory, and simulation, *Hydrol. Earth Syst. Sci.*, *21*, 1063–1076, doi:10.5194/hess-21-1063-2017.

Moebius, F., and D. Or (2012), Interfacial jumps and pressure bursts during fluid displacement in interacting irregular capillaries, *J. Colloid Interface Sci.*, *377*, 406–415, doi:10.1016/j.jcis.2012.03.070.
Morrow, N. R. (1970), Physics and thermodynamics of capillary action in porous media, *Ind. Eng. Chem.*, *62*, 32–56, doi:10.1021/ie50726a006.
Moura, M., E.-A. Fiorentino, K. J. Måløy, G. Schäfer, and R. Toussaint (2015), Impact of sample geometry on the measurements of pressure-saturation curves: Experiments and simulations, *Water Resour. Res.*, *51*, 8900–8926, doi:10.1002/2015WR017196.
Moura, M., K. J. Måløy, and R. Toussaint (2016), Critical behavior in porous media flow, arXiv:1611.04210 [physics.flu-dyn].
Måløy, K. J., L. Furuberg, J. Feder, and T. Jøssang (1992), Dynamics of slow drainage in porous media, *Phys. Rev. Lett.*, *68*, 2161–2164.
Øren, P. E., S. Bakke, and O. J. Arntzen (1998), Extending predictive capabilities to network models, *SPE J.*, *3*, 324–336.
Porter, M. L., D. Wildenschild, G. Grant, and J. I. Gerhard (2010), Measurements and prediction of the relationship between capillary pressure, saturation, and interfacial area in a NAPL-water-glass bead system, *Water Resour. Res.*, *46*, W08512, doi:10.1029/2009WR007786.
Rücker, M., et al. (2015), From connected pathway flow to ganglion dynamics, *Geophys. Res. Lett.*, *42*, 3888–3894, doi:10.1002/2015GL064007.
Saye, R. I., and J. A. Sethian (2011), The Voronoi implicit interface method for computing multiphase physics, *Proc. Natl. Acad. Sci. U.S.A.*, *108*(49), 19,498–19,503, doi:10.1073/pnas.1111557108.
Schlüter, S., S. Berg, M. Rücker, R. T. Armstrong, H.-J. Vogel, R. Hilfer, and D. Wildenschild (2016), Pore-scale displacement mechanisms as a source of hysteresis for two-phase flow in porous media, *Water Resour. Res.*, *52*, 2194–2205, doi:10.1002/2015WR018254.
Seth, S., and N. Morrow (2007), Efficiency of the conversion of work of drainage to surface energy for sandstone and carbonate, *SPE J.*, *10*, 338–347, doi:10.2118/102490-PA.
Sheppard, A. (2015), *Network Generation Comparison Forum*, Digital Rocks Portal, Univ. of Tex., Austin. [Available at https://doi.org/10.17612/P7059V.]
Singh, K., B. Bijeljic, and M. J. Blunt (2016), Imaging of oil layers, curvature and contact angle in a mixed-wet and a water-wet carbonate rock, *Water Resour. Res.*, *52*, 1716–1728, doi:10.1002/2015WR018072.
Wilkinson, D., and J. F. Willemsen (1983), Invasion percolation: A new form of percolation theory, *J. Phys. A: Math. Gen.*, *16*, 3365–3376.
Xu, J., and M. Y. Louge (2015), Statistical mechanics of unsaturated porous media, *Phys. Rev. E*, *92*, 062405, doi:10.1103/PhysRevE.92.062405.
Zacharoudiou, I., and E. S. Boek (2016), Capillary filling and Haines jump dynamics using free energy lattice Boltzmann simulations, *Adv. Water Resour.*, *92*, 43–56, doi:10.1016/j.advwatres.2016.03.013.